Nonreciprocal guided waves in the presence of swift electron beams

Asma Fallah ,¹ Yasaman Kiasat,^{1,*} Mário G. Silveirinha ,² and Nader Engheta ,^{1,†}

1 University of Pennsylvania, Department of Electrical and Systems Engineering, Philadelphia, Pennsylvania 19104, USA

2 University of Lisbon-Instituto Superior Técnico and Instituto de Telecomunicações, Avenida Rovisco Pais, 1, 1049-001 Lisboa, Portugal

(Received 17 November 2020; revised 9 May 2021; accepted 12 May 2021; published 4 June 2021)

Breaking the reciprocity of electromagnetic interactions is of paramount importance in photonic and microwave technologies, as it enables unidirectional power flows and other unique electromagnetic phenomena. Here we explore a method to break the reciprocity of electromagnetic guided waves utilizing an electron beam with a constant velocity. By introducing an effective dynamic conductivity for the beam, we theoretically demonstrate how nonreciprocal guided waves and a one-way propagating regime can be achieved through the interaction of swift electrons with electromagnetic waves in two-dimensional (2D) parallel-plate and three-dimensional (3D) circular-cylindrical waveguides. Unlike the conventional electron beam structures such as traveling wave tubes and electron accelerators, here the goal is neither to generate and/or amplify the wave nor to accelerate electrons. Instead, we study the salient features of nonreciprocity and unidirectionality of guided waves in such structures. The relevant electromagnetic properties such as the modal dispersion, the field distributions, the operating frequency range, and the nonreciprocity strength and its dependence on the electron velocity and number density are presented and discussed. Moreover, we compare the dispersion characteristics of waves in such structures with some electric-current-based scenarios in materials reported earlier. This broadband tunable magnet-free method offers a unique opportunity to have a switchable strong nonreciprocal response in optoelectronics, nanophotonics, and THz systems.

DOI: 10.1103/PhysRevB.103.214303

I. INTRODUCTION

The reciprocity theorem for electromagnetic fields and waves is a generalization of Lord Rayleigh's reciprocity theorem for sound waves [1]. The electromagnetic version of the theorem stems from the seminal work of Lorentz and Helmholtz and is a cornerstone of the Maxwell theory. The Lorentz reciprocity theorem states that in linear time-invariant structures with materials described by symmetric tensors, one can interchange the locations of the source and observer without changing the observed field strength [2-5]. Achieving nonreciprocity has been the subject of research interest for years, offering practical opportunities over the past decades (e.g., Refs. [5–32]). For example, a nonreciprocal response is indispensable for realizing circulators, isolators [5,8,9,14,15,21-23,25,32], optical diodes [6,13,16,24,26], and energy sinks [17,31]. Therefore, there has been a tremendous effort in the development of robust solutions to break reciprocity [4,5,8,9,21,22,32]. The known approaches can, generally, be divided into two categories; (1) solutions that involve DC biasing magnetic field and (2) the magnet-free solutions.

Reciprocity can be broken via magnetically biased gyromagnetic materials (known since the 1950's [33–36]). In addition to its bulkiness, a primary problem with this method

is a fairly weak nonreciprocal response at terahertz and higher frequencies, as a Tesla-level magnetic field results in the cyclotron frequency in the microwave frequency range. Indeed, it is usually impractical to push the cyclotron frequency to the THz range or higher frequencies. Furthermore, large magnetic fields require bulky solenoids, which are challenging to integrate with planar technologies and nanophotonics [37].

Several approaches have been developed to break reciprocity without a biasing magnetic field. For instance, nonlinear effects [6,7,10,13,16,24,26], optomechanical interaction [38–40], spatiotemporally modulated guided-wave structures [9,15,19,21–23,25,32,41], transistor-based metamaterials [11,12,18], and moving media [28,38]. These approaches have their own advantages and constraints (e.g., see Refs. [42–44]).

Recently, several methods explored the possibility of using a drift current in graphene to break the time-reversal symmetry [31,45–48]. The drift current originates a "plasmonic" drag effect that can lead to unidirectional propagation regimes [45,48] and a strong nonreciprocity. The effect of the drift current on the graphene conductivity has been modeled using linear response (Kubo's) theory either through a nonequilibrium Fermi distribution or through a suitable interaction Hamiltonian [47–49]. The effect of drift current has also been studied in semiconductors for a purpose of parametric amplification [50], however, comparing with graphene the velocity of the electrons is constrained by the lower mobility in semiconductors. Moreover, the nonreciprocity due to electric currents in metals has also been investigated [27], but here the velocity of electrons is extremely low, resulting in weak

^{*}Present address: 210 Locust St, 16E, Philadelphia, Pennsylvania 19106, USA, yasaman.kiassat@gmail.com

[†]engheta@seas.upenn.edu

nonreciprocity. The nonreciprocal response stems from the fact that the electric current is odd under a time reversal. Although graphene may exhibit high electron mobility, even in this case the drift velocity is fundamentally limited by graphene's Fermi velocity $v_F = c/300$ [51]. The nonreciprocity strength is determined by the Doppler shift v_0k (k is the plasmons wave number, parallel or antiparallel to the direction of motion of electrons, and v_0 is the drift velocity). A strong nonreciprocity requires that the Doppler shift v_0k must be a significant fraction of the operating frequency. Therefore, the nonreciprocal response in graphene is constrained by its Fermi velocity (and in semiconductors and metals such nonreciprocity is even much weaker). Moreover, large drift velocities are very challenging to achieve and can cause heating and compromise the integrity of the graphene sheet, solid-state, and metallic materials.

In this work, we explore a different tunable method to break the reciprocity. Rather than considering that the electrons move in a solid-state material, as in graphene, or in metal, here we suppose that the swift electrons are accelerated in a vacuum to constant high velocities. This approach tackles the aforementioned challenges of achieving high electron velocities. For example, in the cathodoluminescence microscopes, a 30-keV electron beam has an electron velocity of around $v_0 = c/3$ [52,53]. Furthermore, as we show here, the interaction of a beam of swift electrons with guided electromagnetic waves around the electron beam can lead to extreme nonreciprocity at high frequencies and relatively wide bandwidths. It is worth noting that although the interaction of electromagnetic waves with electron beams has been studied for decades in microwave generators such as the traveling wave tubes [54] and in electron accelerator structures [55], the goal here is neither to generate or amplify waves nor to accelerate electrons. Instead, we investigate quantitatively how tunable broadband nonreciprocity can be achieved in guided waves in presence of electron beams with constant velocities. It should also be noted that the current state-of-art technology may enable the integration on a chip of the circuitry required to generate the electron beam [56,57].

We study the interactions between the swift electrons and the transverse-magnetic TM electromagnetic mode in two illustrative cases; (1) a parallel-plate waveguide containing an electron sheet (planar beam) with electron velocity v_0 to demonstrate the theory for the two-dimensional (2D) scenario and (2) a hollow metallic cylindrical uniform waveguide with a circular cross section having a collimated electron beam (pencil beam) along its axis, as a possible case for future experimentation. We theoretically study the dispersion relations for these two cases and examine the nonreciprocal response of the corresponding waveguides for various electron beam constant velocities. Our proposal can obviously be extended to other waveguide geometries. In the following, a time-harmonic convention of the form $e^{i\omega t}$, with ω as the operating angular frequency, is assumed.

It is worth noting here that the electron beam is assumed to be associated with a steady flow (stationary current) of electrons in vacuum inside the guided-wave structure with cross section invariant along the axis, and consequently, it does not lead to the emission of Cherenkov type radiation [59] or Smith-Purcell type radiation [60] and creates only a static-type field distribution.

The current density of the electron beam can, however, be perturbed by a high-frequency (external) electromagnetic field propagating in the guide. The perturbation can be characterized using a transport equation obtained with the Boltzmann's formalism (see Eq. S1 [58]) [61]. It is worth noting that the Boltzmann equation, which is usually utilized for charged carriers in materials, has been applied here to the stream of electrons in vacuum. (In the Supplemental Material, we have also included another derivation that regards the electron beam as a polarizable rod, rather than as a bulk material; the two approaches lead to the same physics.) It is possible to linearize the continuity (see Eq. S2 [58]) and the transport equations. The electron density and the electron velocity are split into the equilibrium (DC) part and time-harmonically varying (AC) part due to the perturbation by an external field. The AC terms are treated as small perturbations of the corresponding DC values (e.g., products of the AC parts of two quantities are neglected). In this manner, it is possible to show that the longitudinal AC current density (Eqs. S3 and S6 [58]) is linked to the AC field as follows:

$$J_{z} = \frac{(q^{2}n_{0}/m)\omega E_{z}}{i[(\omega - v_{0}k_{z})^{2} - k_{z}^{2}\beta] + \tau^{-1}\omega},$$
(1)

where the electron beam is assumed to travel along the z axis [Fig. 1(a)], E_z and k_z are, respectively, the longitudinal z components of the time-varying electric field at the electron beam and wave vector of the TM mode of the waveguide, and n_0 , m, q, v_0 are all constant quantities, denoting the equilibrium electron number density, electron rest mass, the electron charge, and constant electron velocity, respectively. Furthermore, τ and β represent the average scattering time and diffusion coefficient (e.g., due to electron-electron repulsion), respectively. We point out that Eq. (1) describes the effective dynamic conductivity of the electron beam. In other words, it gives the effective medium (macroscopic) conductivity for the time-varying monochromatic parts of the electric field and current density. Since the electron beam thickness is assumed to be very small, the transverse components of the electric field (if any) do not interact with the beam. Thus, only the longitudinal component of electric field interacts noticeably with the electrons. It is worth noting that for velocities very close to the speed of light c, a relativistic correction (Lorentz factor) for the electron mass should be considered [62]. However, in our results reported in this paper, the maximum velocity we consider is c/3, for which the Lorentz factor, being 1.0607, is still very close to unity. To highlight the main features of the guided modes, in the following we neglect the diffusion and scattering terms. This leads to

$$J_z = \frac{q^2 n_0 \omega E_z}{i m (\omega - v_0 k_z)^2} = -i \omega \epsilon_0 (\frac{\omega_p}{\tilde{\omega}})^2 E_z, \tag{2}$$

where $\omega_p^2 \equiv q^2 n_0/m\epsilon_0$ and $\tilde{\omega} \equiv (\omega - v_0 k_z)$ which is the Doppler-shifted frequency in the frame co-moving with the electrons. Equation (2) reveals that from the point of view of the dynamic (i.e., AC part) electromagnetic signal, the effective permittivity of the beam (in the laboratory frame) is alike to a Drude model, with the frequency term replaced by

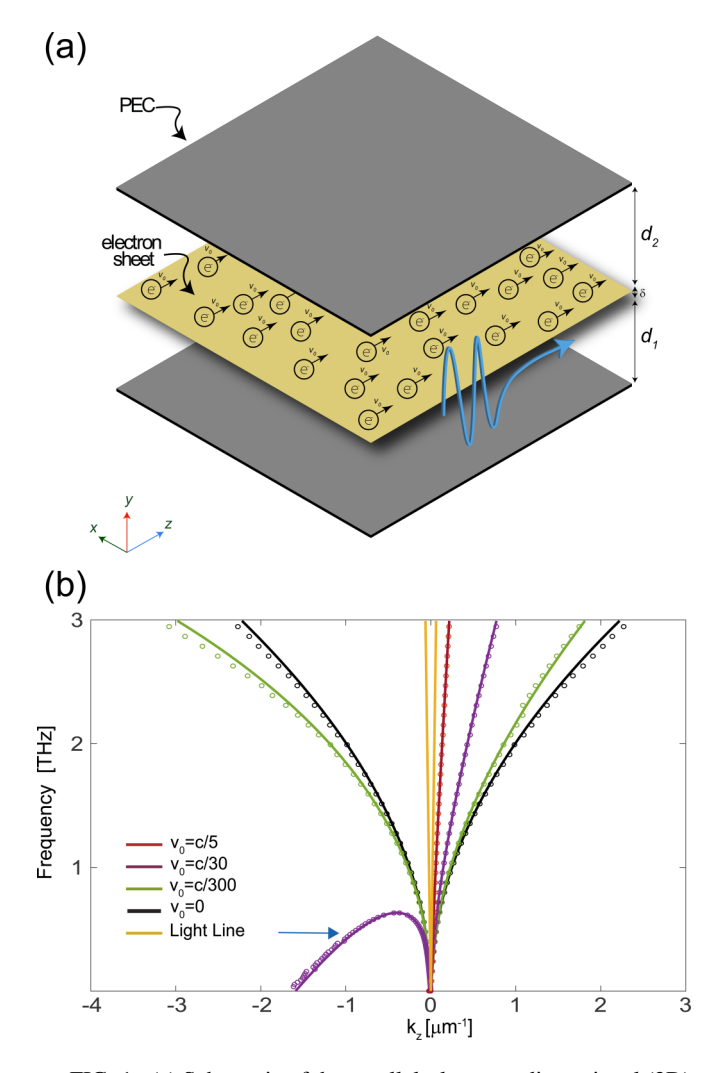


FIG. 1. (a) Schematic of the parallel-plate two-dimensional (2D) waveguide containing a two-dimensional (planar) electron beam (yellow region). (b) Dispersion diagram for the TM_{10} mode of the parallel plate waveguide for various electron velocities v_0 . Solid lines: analytical results; circles: simulation results. The blue arrow indicates the frequency f = 0.48 THz corresponding to the electric field profiles shown in the Supplemental Material Fig. S1 [58].

 $\tilde{\omega}$. In particular, the model predicts that the beam response is different for oppositely-signed values of k_z , i.e., for the two opposite directions of guided-wave propagation for a fixed operating frequency. This property is a clear fingerprint of break of reciprocity.

II. MODAL CHARACTERISTICS OF PARALLEL-PLATE METALLIC WAVEGUIDES WITH AN ELECTRON SHEET

To highlight the consequences of the nonreciprocal interactions between the beam and the wave, first we consider a (2D) parallel-plate waveguide, which, without loss of generality and for the sake of simplicity, is assumed to be made of perfect electric conducting (PEC) plates. [For this 2D scenario the electron beam is in the *xoz* plane (planar beam), and thickness of the beam along *y* is assumed to be negligible (thin planar beam).] The electron beam travels in a direction parallel to the PEC plates, as shown in Fig. 1(a). The distance

between the metallic plates is d, whereas the distances between the planar beam and the bottom and top PEC plates are d_1 and d_2 , respectively. Solving Maxwell's equations and applying the appropriate boundary conditions at the waveguide's plates and at the electron sheet, the modal dispersion and the corresponding electromagnetic field distributions can be analytically derived (details are shown in the Supplemental Material). The electron beam is surrounded by a vacuum and its thickness δ is considered to be electrically thin enough so E_z is assumed to be approximately uniform across the beam.

For the TM mode with E_z , E_y , and H_x field components and denoting $k_0^2 \equiv \omega^2 \mu_0 \epsilon_0$ and $k_y^2 \equiv k_0^2 - k_z^2$, the dispersion relation is given by

$$\frac{q^2 n_0' / m \epsilon_0}{\tilde{\omega}^2} = -\frac{1}{k_v \tan(k_v d_1)} - \frac{1}{k_v \tan(k_v d_2)}.$$
 (3)

Note that since δ is infinitesimally small, here for the planar case we define a surface density for the electron beam to be $n_0' = n_0 \delta$ which is expressed as an electron number density per unit area.

Figure 1(b) shows the calculated dispersion diagrams, for $d_1 = d_2 = d/2$ with d = 0.05 mm, and $n'_0 = 10^{17}$ m⁻². The solid lines represent the dispersion curves obtained from our analytical expression [Eq. (3)], while the circles show the results of numerical simulations done using the commercially available COMSOL Multiphysics® [64] (see the Supplemental Material for the simulation methods [58]). The simulation and analytical results show that the higher the electron velocity is, the larger is the spectral asymmetry and the difference between the wave numbers of the guided waves (the TM₁₀ mode) propagating in +z and -z directions. Thus, the simulation and analytical results show unequivocally that the motion of electrons in the electron beam inside the guide can result in Fresnel-type drag of the electromagnetic waves and lead to a very strong nonreciprocity even at high frequencies. In order to highlight the strength of nonreciprocity in our high-velocity electron beam structures, in Fig. 2 as a parametric study we present dispersion diagrams for several values of electron number densities and electron velocities, some of which are the parameters for the cases of GaAs $(n'_0 =$ 10^{15} m^{-2} , $v_0 = 5 \times 10^4 \text{ m/s [50]}$), InSb $(n'_0 = 4 \times 10^{15} \text{ m}^{-2})$, $v_0 = 3.7 \times 10^3 \text{ m/s [63]}$), and graphene $(n'_0 = 10^{16} \text{ m}^{-2})$, $v_0 = 10^{16} \text{ m}^{-2}$ v_F [45]) reported in the literature. In this figure, panels (b) and (c) show the zoom-in versions of panels (a) and (b), respectively, around the origin. It is important to note that since in our structure the electron velocity can be much higher than those in GaAs, InSb, and graphene (as here the electron velocity is not constrained by the mobility of electrons in those materials), much stronger nonreciprocity and unidirectionality can be obtained. Comparison for the case of cylindrical waveguides is discussed in the following section. As shown in Fig. 1(b) and Fig. 2, at some frequencies the dispersion diagrams bend in opposite directions (up or down) depending on the sign of k_z . The turning points depend on the electron velocity among other parameters. Clearly, as can be seen in Fig. 2 the strength of nonreciprocity can be tailored with the electron velocity and the electron density. This is a rather unique and attractive feature of this magnetic-free

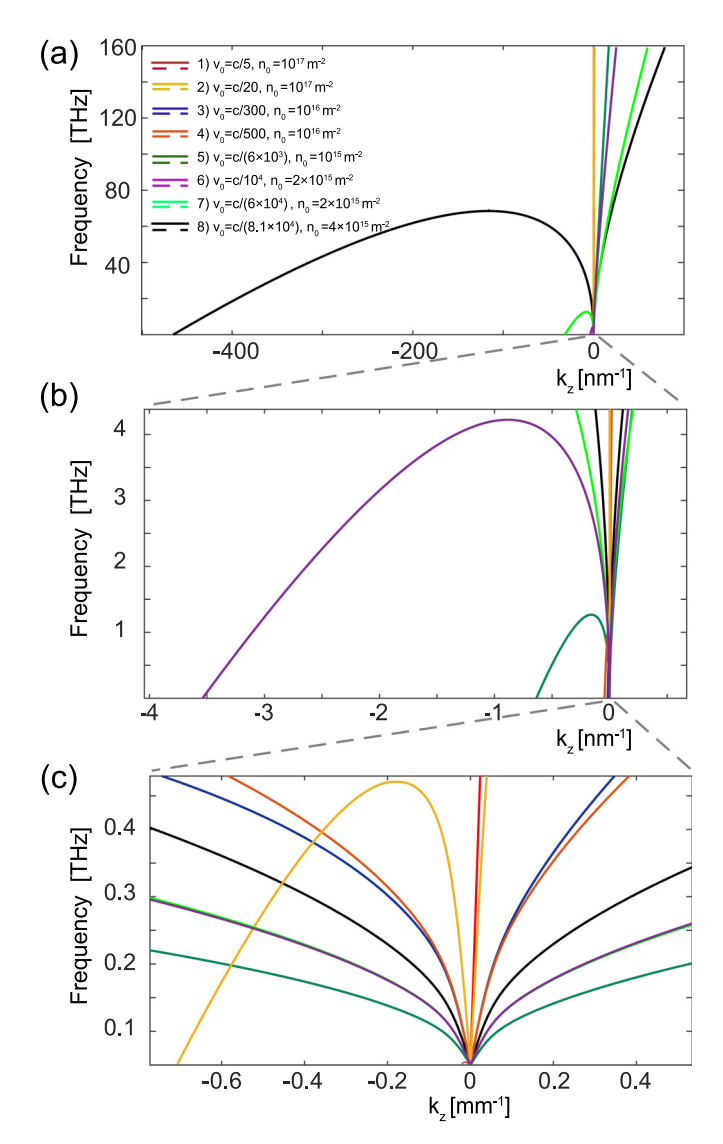


FIG. 2. Comparative study: Dispersion diagrams of the parallel plate waveguides with thickness of d=0.05 mm and various values for the electron beam properties (n_0' and v_0). Three of the eight sets of parameters are for specific materials and five others are various parameters arbitrarily chosen. Cases (3), (5), and (8) are dispersion diagram of this waveguide loaded with graphene [45], GaAs [50], and InSb [63], respectively. From panel (a) towards panel (c), zoomed-in plots near the origin are shown.

nonreciprocal platform where the electron flow with constant velocity breaks the time reversal symmetry.

In addition, in Fig. S1 [58] of Supplemental Material we have depicted time snapshots of the y and z components of the electric field distributions at f = 0.48 THz when $v_0 = c/30$. It is worth mentioning that at this frequency a hollow waveguide with the same thickness would be well below the cutoff frequency for the TM₁₀ mode if we did not have the moving electron beam. The plasma type response of the electron beam suppresses the cutoff of this mode, even in the limit $v_0 = 0^+$. As is seen in Fig. 1(a), at the selected frequency of operation, there are three allowed values for the longitudinal wave numbers: one positive k_z and two negative k_z values. In Fig. S1, we present the modal field distributions for the

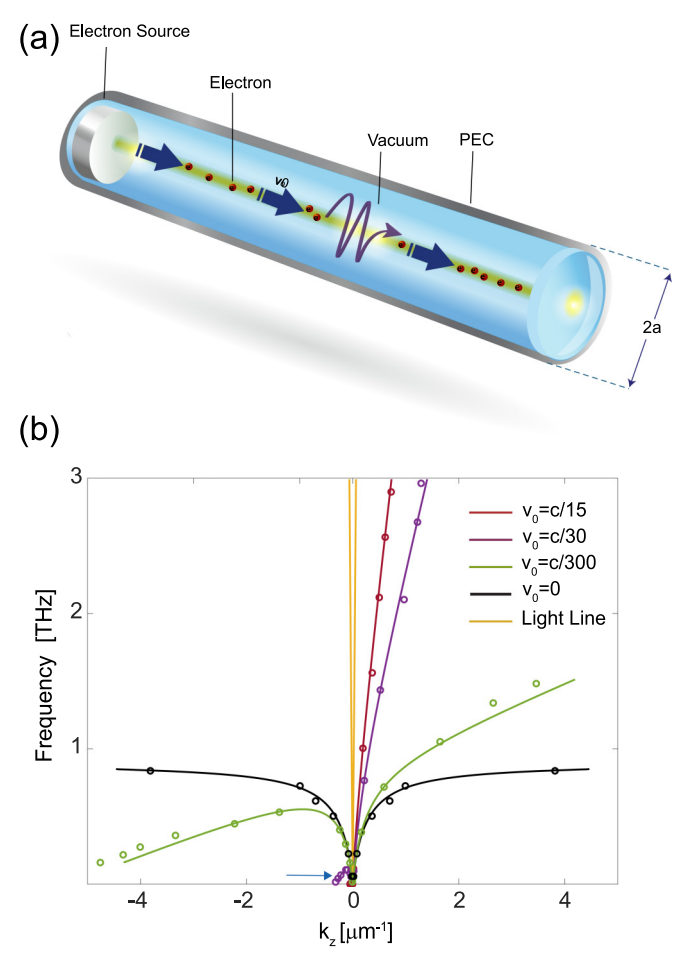


FIG. 3. (a) Schematic of the circular cylindrical waveguide with an axial electron pencil beam; the beam trajectory is represented by the green line. (b) Dispersion diagram for the TM_{10} mode of cylindrical waveguide for various beam velocities v_0 . Solid lines: analytical results; circles: simulation results. The blue arrow marks the frequency f = 0.08 THz corresponding to the electric field profiles shown in Fig. S2 [58].

three possible k_z values at 0.48 THz. Note that one of the negative k_z modes is a backward wave. From Fig. S1, it is evident that the field profiles are rather different for the +z and -z directions of propagation, which is another manifestation of the nonreciprocity of the system. This result can also be intuitively explained by the fact that according to Eq. (2) the effective dynamic conductivity of the electron beam explicitly depends on k_z when $v_0 \neq 0$.

III. MODAL CHARACTERISTICS OF A HOLLOW METALLIC CIRCULAR-CYLINDRICAL WAVEGUIDE WITH AN ON-AXIS ELECTRON BEAM

Next, we analyze the case of the 3D hollow circularcylindrical waveguide of radius a with PEC wall, with a pencil-type electron beam of radius b flowing with constant velocity v_0 along this waveguide axis [Fig. 3(a)]. The dynamic (i.e., AC part) current density in the electron beam is still given by Eq. (2), but now we use n_0 which is number density per unit volume. To investigate the nonreciprocal behavior of this system, we analytically derived the dispersion relation for the TM_{10} mode. (As an aside we point out that here we use the terminology TM_{10} , even though the radial variations of the field quantities do not have the "Bessel-function-like behavior," but instead they have the modified-Bessel-function behavior.) Having $k_r^2 \equiv k_0^2 - k_z^2$, the dispersion relation of the TM_{10} mode supported by the system in the limit of $b \ll \lambda$ is determined by

$$\left(\frac{\omega_p}{\tilde{\omega}}\right)^2 \approx -\frac{2}{k_r b} \frac{C(k_r a) J_1(k_r b) + Y_1(k_r b)}{C(k_r a) J_0(k_r b) + Y_0(k_r b)} + 1,$$
(4)

where $C(k_r a) \equiv -Y_0(k_r a)/J_0(k_r a)$ with J_n and Y_n being the Bessel functions of the first and second kind and a is the radius of the cylindrical waveguide.

Figure 3(b) depicts the dispersion diagram (solid lines: analytical results, circles: numerical results) of the TM₁₀ mode for several electron velocities v_0 ($v_0 = c/15, c/30, c/300$) and considering $n_0 = 10^{22} \text{ m}^{-3}$, $a = 38 \,\mu\text{m}$, and $b = 3.8 \,\mu\text{m}$. As before, it is found that the electron flow in the channel results in large spectral asymmetry and strong nonreciprocity. For instance, for $v_0 = c/300$ and for frequencies above 0.4 THz the wave can experience highly nonreciprocal behavior. Similar to the parallel plate case, there is also a "turning-point frequency" where the group velocity vanishes. For frequencies below the turning point, the guide supports modes with a negative k_z value. It is worth noting that for the electron beam parameters of Fig. 3, the total current is much larger than the currents than can be provided by some of the conventional electron beam devices such as the cathodoluminescence microscope. The reason we use a large current is to highlight more clearly the impact of the electron beam on the wave propagation. In a cathodoluminescence microscope the typical currents are in the range of 10 pA and 10 nA (e.g., see Refs. [52,53]) for electrons with velocity c/3. Hence, to show the compatibility of our proposal with commercially available electron beam generators along with other practical and theoretical cases, we conducted a parametric study for different scenarios. Figure 4 demonstrates dispersion diagrams of the cylindrical waveguide case with various values for the electron beam's properties such as radius, velocity, and density. This study includes four specific practical cases such as metallic wires [20,27], cathodoluminesence (CL) beam [52,53], and an electron gun [65], along with four other cases with selected arbitrary parameter values. It is important to note that for the cylindrical geometries discussed here, the asymptotic line of the dispersion curves is $(\omega - v_0 k_z) = \omega_p$, which shows that its intersection with the vertical axis is at the plasma frequency and its slope is the velocity of electrons. This implies that for higher electron velocity and/or lower plasma frequency we can achieve stronger nonreciprocity and unidirectionality. In order to highlight this point, we have considered and shown several cases with different n_0 (thus different plasma frequencies) and different v_0 . In Fig. 4, the dashed curves represent the asymptotic lines. Comparison among the various cases (including the four practical cases mentioned above) is informative in this figure. For example in the metal case [27] the plasma frequency is very high and the electron velocity is very low, and consequently the electric-current-based nonreciprocity in metals is very weak. As we decrease the plasma

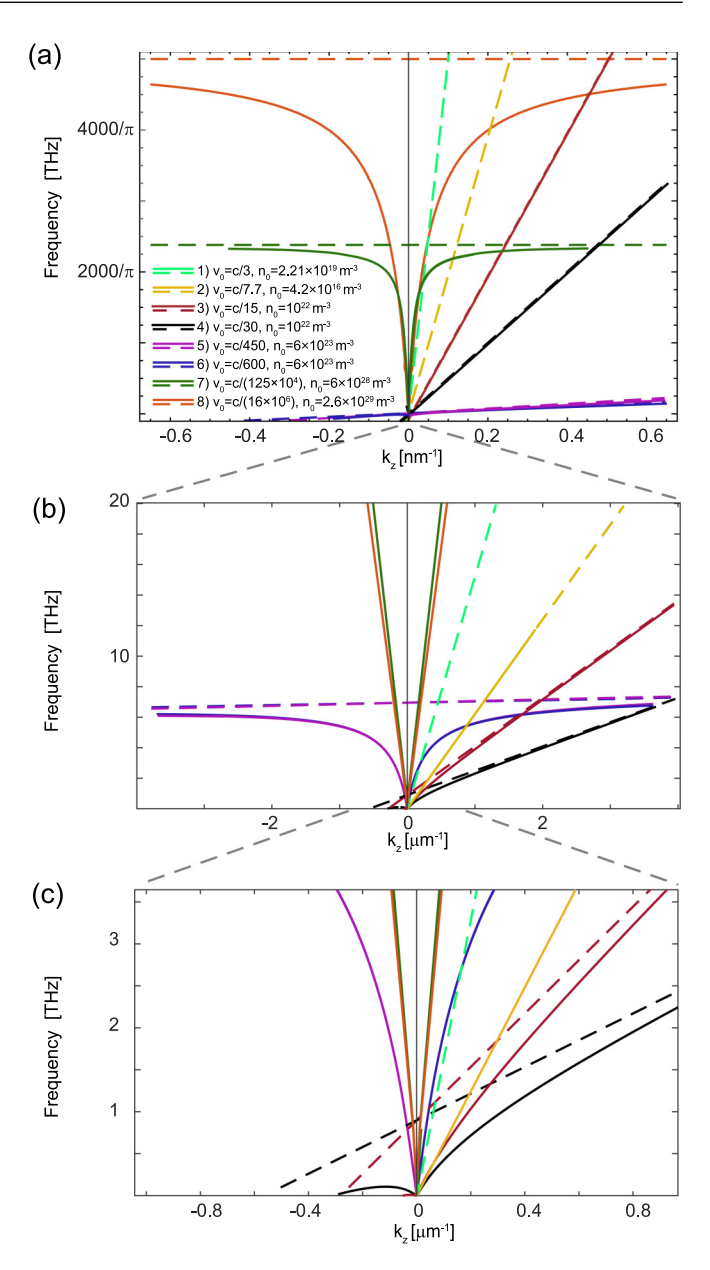


FIG. 4. Comparative study: Dispersion diagrams of the cylindrical waveguides with an outer radius of $a=40~\mu\mathrm{m}$ and various values for the electron beam properties $(n_0, v_0, \text{and } b)$. Four of the eight sets of parameters are for specific cases of materials and electron beams and four others are parameters arbitrarily selected. Cases (1), (2), (7), and (8) are dispersion diagrams of the cylindrical waveguide containing the cathodoluminescence beam [52,53], an electron gun (EM 503) [65], gold rod [20], and a metal [27], respectively. Solid and dashed lines represent the dispersion diagrams and their asymptotes, respectively. The radii of the electron beams for cases (1) and (2) are 3 nm and 1.5 μ m, for (3–6) 3.8 μ m, and for (7) and (8) 0.1 μ m and 20 nm, respectively. From panel (a) towards panel (c), zoomed-in plots near the origin are shown.

frequency and increase the electron velocity, i.e., for cases of interest to us, e.g., for the CL and electron gun beams, the nonreciprocal response and unidirectionality become much stronger over a wide range of frequencies. Interestingly, in these cases, the response can be strongly nonreciprocal such

that the turning point of the modal dispersion occurs at very low frequencies, yielding thereby a broadband regime of unidirectional propagation.

It is worth noting that in all these cases, the average longitudinal distance (d_{avg}) between neighboring electrons in the beam must be less than the wavelength of guided wave along the beam so that the effective theory remains valid. Here one can consider $d_{\text{avg}} = 1/n_0 A$ where $A = \pi b^2$ is the cross-sectional area of the electron beam. In other words, the frequency of operation should stay below the frequency for which the longitudinal wave number k_z is less than $k_{avg} =$ $2\pi/d_{\rm avg}=2\pi n_0 A$. For instance, for the electron gun (EM 503) the $k_{\rm avg}$ is 1.86 $\mu {\rm m}^{-1}$, therefore frequencies with wave number smaller than 1.86 μm^{-1} are applicable. The average distance of cases (1) through (8) in Fig. 5 [cases (3,4) and (5,6) have the same number density and same radius, hence same k_{avg}] are 3.92 mm⁻¹, 1.86 μ m⁻¹, 2.85 pm⁻¹, 170 pm⁻¹, 11844 pm⁻¹, and 2052 pm⁻¹, respectively. Hence, as it is demonstrated in Fig. 4, for the electron gun and CL cases, dispersion curves (solid lines) have been stopped at the frequencies (11.5 THz and 62.3 GHz, respectively) beyond which the effective medium theory will not be valid.

Supplemental Fig. S2 [58] shows the time snapshots of the r and z components of the electric field distributions at f=0.08 THz and $v_0=c/30$. As before, the fields are highly concentrated near the electron beam. We should also note that the nonreciprocal guided mode is somewhat alike to a guided surface plasmon concentrated near the electron beam, and its propagation is little affected by the outer wall of the waveguide. However, the presence of the waveguide wall ensures that only this nonreciprocal TM_{10} mode can propagate and that the higher-order modes are below the cutoff. See the Supplemental Material for the dispersion curves for different waveguide radii [58].

IV. CONCLUSIONS

In conclusion, in this paper we have discussed a mechanism to break the electromagnetic reciprocity at relatively high frequencies that exploits the interaction of electromagnetic guided waves with electron beams with moderately high constant velocity. We have illustrated the concept by calculating the dispersion of the guided modes of two different hollow metallic waveguides containing a moving electron beam surrounded by a vacuum. Our theoretical analysis has shown that the guided modes can be effectively dragged by the swift electrons and that the light-matter interactions in the guide enable unidirectional propagation regimes and a strong nonreciprocity. We have compared the case of high-velocity electron beams with some of the practical scenarios and have concluded that the electron beams can provide much stronger nonreciprocity and unidirectionality. The proposed method opens up new perspectives and possibilities in controlling and manipulating the direction of flow of electromagnetic waves in optoelectronics, THz systems, and nanophotonics networks, as the nonreciprocity strength is not constrained by the material properties. This form of nonreciprocity can be applicable to other general guided-wave structures with hollow cores such as holey fibers.

ACKNOWLEDGMENTS

The authors express their thanks to Miguel Camacho of the University of Pennsylvania for valuable discussions. This work is supported in part by the National Science Foundation (NSF) Emerging Frontiers in Research and Innovations (EFRI) Program Grant No. 1741693. M.G.S. was supported by Instituto de Telecomunicações under Project No. UID/EEA/50008/2020.

- [1] J. W. Strutt and B. Rayleigh, *The Theory of Sound* (Dover, New York, 1945).
- [2] I. Lindell, Methods for Electromagnetic Field Analysis, IEEE/OUP Series on Electromagnetic Wave Theory (IEEE, New York, 1995).
- [3] D. H. Staelin, A. W. Morgenthaler, and J. A. Kong, *Electro-magnetic Waves* (Pearson Education India, Englewood Cliffs NJ, 1994).
- [4] L. Deák and T. Fülöp, Reciprocity in quantum, electromagnetic and other wave scattering, Ann. Phys. **327**, 1050 (2012).
- [5] C. Caloz, A. Alù, S. Tretyakov, D. Sounas, K. Achouri, and Z.-L. Deck-Léger, Electromagnetic Nonreciprocity, Phys. Rev. Appl. 10, 047001 (2018).
- [6] K. Gallo, G. Assanto, K. R. Parameswaran, and M. M. Fejer, All-optical diode in a periodically poled lithium niobate waveguide, Appl. Phys. Lett. 79, 314 (2001).
- [7] M. Soljačić, C. Luo, J. D. Joannopoulos, and S. Fan, Nonlinear photonic crystal microdevices for optical integration, Opt. Lett. 28, 637 (2003).
- [8] Z. Yu, G. Veronis, Z. Wang, and S. Fan, One-Way Electromagnetic Waveguide Formed at the Interface Between a Plasmonic

- Metal Under a Static Magnetic Field and a Photonic Crystal, Phys. Rev. Lett. **100**, 023902 (2008).
- [9] Z. Yu and S. Fan, Complete optical isolation created by indirect interband photonic transitions, Nat. Photon. 3, 91 (2009).
- [10] H. Ramezani, T. Kottos, R. El-Ganainy, and D. N. Christodoulides, Unidirectional nonlinear Pt-symmetric optical structures, Phys. Rev. A 82, 043803 (2010).
- [11] T. Kodera, D. L. Sounas, and C. Caloz, Nonreciprocal magnetless CRLH leaky-wave antenna based on a ring metamaterial structure, IEEE Anten. Wireless Propag. Lett. 10, 1551 (2011).
- [12] T. Kodera, D. L. Sounas, and C. Caloz, Artificial faraday rotation using a ring metamaterial structure without static magnetic field, Appl. Phys. Lett. 99, 031114 (2011).
- [13] I. V. Shadrivov, V. A. Fedotov, D. A. Powell, Y. S. Kivshar, and N. I. Zheludev, Electromagnetic wave analogue of an electronic diode, New J. Phys. 13, 033025 (2011).
- [14] L. Bi, J. Hu, P. Jiang, D. H. Kim, G. F. Dionne, L. C. Kimerling, and C. Ross, On-chip optical isolation in monolithically integrated non-reciprocal optical resonators, Nat. Photon. 5, 758 (2011).

- [15] H. Lira, Z. Yu, S. Fan, and M. Lipson, Electrically Driven Nonreciprocity Induced by Interband Photonic Transition on a Silicon Chip, Phys. Rev. Lett. 109, 033901 (2012).
- [16] L. Fan, J. Wang, L. T. Varghese, H. Shen, B. Niu, Y. Xuan, A. M. Weiner, and M. Qi, An all-silicon passive optical diode, Science 335, 447 (2012).
- [17] O. Luukkonen, U. K. Chettiar, and N. Engheta, One-way waveguides connected to one-way loads, IEEE Anten. Wireless Propag. Lett. 11, 1398 (2012).
- [18] Z. Wang, Z. Wang, J. Wang, B. Zhang, J. Huangfu, J. D. Joannopoulos, M. Soljačić, and L. Ran, Gyrotropic response in the absence of a bias field, Proc. Natl. Acad. Sci. USA 109, 13194 (2012).
- [19] D. L. Sounas, C. Caloz, and A. Alu, Giant non-reciprocity at the subwavelength scale using angular momentum-biased metamaterials, Nat. Commun. 4, 2407 (2013).
- [20] A. Davoyan and N. Engheta, Electrically controlled one-way photon flow in plasmonic nanostructures, Nat. Commun. 5, 5250 (2014).
- [21] R. Fleury, D. L. Sounas, C. F. Sieck, M. R. Haberman, and A. Alù, Sound isolation and giant linear nonreciprocity in a compact acoustic circulator, Science 343, 516 (2014).
- [22] N. A. Estep, D. L. Sounas, J. Soric, and A. Alù, Magnetic-free non-reciprocity and isolation based on parametrically modulated coupled-resonator loops, Nat. Phys. 10, 923 (2014).
- [23] D. L. Sounas and A. Alú, Angular-momentum-biased nanorings to realize magnetic-free integrated optical isolation, ACS Photon. 1, 198 (2014).
- [24] A. M. Mahmoud, A. R. Davoyan, and N. Engheta, All-passive nonreciprocal metastructure, Nat. Commun. 6, 8359 (2015).
- [25] D. L. Sounas and A. Alù, Non-reciprocal photonics based on time modulation, Nat. Photon. 11, 774 (2017).
- [26] D. L. Sounas and A. Alù, Nonreciprocity based on nonlinear resonances, IEEE Anten. Wireless Propag. Lett. 17, 1958 (2018).
- [27] K. Bliokh, F. J. Rodríguez-Fortuño, A. Bekshaev, Y. Kivshar, and F. Nori, Electric-current-induced unidirectional propagation of surface plasmon-polaritons, Opt. Lett. 43, 963 (2018).
- [28] Y. Mazor and A. Alù, Nonreciprocal hyperbolic propagation over moving metasurfaces, Phys. Rev. B 99, 045407 (2019).
- [29] Y. Li, Y.-G. Peng, L. Han, M.-A. Miri, W. Li, M. Xiao, X.-F. Zhu, J. Zhao, A. Alù, S. Fan *et al.*, Anti–parity-time symmetry in diffusive systems, Science **364**, 170 (2019).
- [30] S. A. Mann, D. L. Sounas, and A. Alù, Broadband delay lines and nonreciprocal resonances in unidirectional waveguides, Phys. Rev. B 100, 020303(R) (2019).
- [31] D. E. Fernandes and M. G. Silveirinha, Topological Origin of Electromagnetic Energy Sinks, Phys. Rev. Appl. 12, 014021 (2019).
- [32] A. Mock, D. Sounas, and A. Alù, Magnet-free circulator based on spatiotemporal modulation of photonic crystal defect cavities, ACS Photon. 6, 2056 (2019).
- [33] B. Lax, K. J. Button, and L. M. Roth, Ferrite phase shifters in rectangular wave guide, J. Appl. Phys. 25, 1413 (1954).
- [34] A. Fox, S. Miller, and M. Weiss, Behavior and applications of ferrites in the microwave region, Bell Syst. Tech. J. 34, 5 (1955).
- [35] K. Button and B. Lax, Theory of ferrites in rectangular waveguides, IRE Trans. Anten. Propag. 4, 531 (1956).

- [36] J. Brion, R. Wallis, A. Hartstein, and E. Burstein, Theory of Surface Magnetoplasmons in Semiconductors, Phys. Rev. Lett. 28, 1455 (1972).
- [37] E. P. Furlani, Permanent Magnet and Electromechanical Devices: Materials, Analysis, and Applications (Academic Press, New York, 2001).
- [38] S. Lannebere and M. G. Silveirinha, Wave instabilities and unidirectional light flow in a cavity with rotating walls, Phys. Rev. A 94, 033810 (2016).
- [39] S. Weis, R. Rivière, S. Deléglise, E. Gavartin, O. Arcizet, A. Schliesser, and T. J. Kippenberg, Optomechanically induced transparency, Science 330, 1520 (2010).
- [40] M. Hafezi and P. Rabl, Optomechanically induced nonreciprocity in microring resonators, Opt. Express 20, 7672 (2012).
- [41] P. A. Huidobro, E. Galiffi, S. Guenneau, R. V. Craster, and J. Pendry, Fresnel drag in space-time-modulated metamaterials, Proc. Natl. Acad. Sci. USA 116, 24943 (2019).
- [42] Y. Shi, Z. Yu, and S. Fan, Limitations of nonlinear optical isolators due to dynamic reciprocity, Nat. Photon. 9, 388 (2015).
- [43] D. L. Sounas and A. Alù, Fundamental bounds on the operation of fano nonlinear isolators, Phys. Rev. B **97**, 115431 (2018).
- [44] D. L. Sounas and A. Alu, Time-Reversal Symmetry Bounds on the Electromagnetic Response of Asymmetric Structures, Phys. Rev. Lett. 118, 154302 (2017).
- [45] T. A. Morgado and M. G. Silveirinha, Drift-induced unidirectional graphene plasmons, ACS Photon. 5, 4253 (2018).
- [46] D. Correas-Serrano and J. S. Gomez-Diaz, Nonreciprocal and collimated surface plasmons in drift-biased graphene metasurfaces, Phys. Rev. B 100, 081410(R) (2019).
- [47] T. A. Morgado and M. G. Silveirinha, Negative Landau Damping in Bilayer Graphene, Phys. Rev. Lett. 119, 133901 (2017).
- [48] D. S. Borgnia, T. V. Phan, and L. S. Levitov, Quasi-relativistic doppler effect and non-reciprocal plasmons in graphene, arXiv:1512.09044.
- [49] B. Van Duppen, A. Tomadin, A. N. Grigorenko, and M. Polini, Current-induced birefringent absorption and non-reciprocal plasmons in graphene, 2D Mater. 3, 015011 (2016).
- [50] O. Sydoruk, R. Syms, and L. Solymar, Amplifying mirrors for terahertz plasmons, J. Appl. Phys. **112**, 104512 (2012).
- [51] V. E. Dorgan, M.-H. Bae, and E. Pop, Mobility and saturation velocity in graphene on SiO₂, Appl. Phys. Lett. 97, 082112 (2010).
- [52] E. S. Barnard, T. Coenen, E. J. R. Vesseur, A. Polman, and M. L. Brongersma, Imaging the hidden modes of ultrathin plasmonic strip antennas by cathodoluminescence, Nano Lett. 11, 4265 (2011).
- [53] A. Polman, M. Kociak, and F. J. G. de Abajo, Electron-beam spectroscopy for nanophotonics, Nat. Mater. 18, 1158 (2019).
- [54] J. Pierce, Theory of the beam-type traveling-wave tube, Proc. IRE **35**, 111 (1947).
- [55] M. Martins and T. Silva, Electron accelerators: History, applications, and perspectives, Radiat. Phys. Chem. 95, 78 (2014).
- [56] F. Liu, L. Xiao, Y. Ye, M. Wang, K. Cui, X. Feng, W. Zhang, and Y. Huang, Integrated cherenkov radiation emitter eliminating the electron velocity threshold, Nat. Photon. 11, 289 (2017).
- [57] N. V. Sapra, K. Y. Yang, D. Vercruysse, K. J. Leedle, D. S. Black, R. J. England, L. Su, R. Trivedi, Y. Miao, O. Solgaard et al., On-chip integrated laser-driven particle accelerator, Science 367, 79 (2020).

- [58] See Supplemental Material http://link.aps.org/supplemental/ 10.1103/PhysRevB.103.214303 for detailed proof of an electron beam's dynamic conductivity model as well as the effective polarizability model of the electron beam, derivation of the dispersion relations and field distributions, and the numerical simulation methods, along with influence of the outer radius of the cylindrical waveguide.
- [59] J. A. Kong, Electromagnetic Wave Theory (John Wiley & Sons, New York, 1986).
- [60] S. J. Smith and E. Purcell, Visible light from localized surface charges moving across a grating, Phys. Rev. **92**, 1069 (1953).

- [61] R. E. Collin, Foundations for Microwave Engineering (John Wiley & Sons, New York, 2007).
- [62] J. D. Jackson, *Classical Electrodynamics*, 3rd ed. (Wiley, New York, 1999).
- [63] O. Sydoruk, V. Kalinin, and L. Solymar, Terahertz instability of optical phonons interacting with plasmons in two-dimensional electron channels, Appl. Phys. Lett. 97, 062107 (2010).
- [64] COMSOL Multiphysics® v. 5.4. www.comsol.com. COMSOL AB, Stockholm, Sweden.
- [65] STAIB Instruments Inc, www.staibinstruments.com. STAIB Instruments, Virginia, USA.